

Modeling the Effect of C/O Ratio on Complex Carbon Chemistry in Cold Molecular Clouds

ALEX N. BYRNE,¹ CHRISTOPHER N. SHINGLEDECKER,² EDWIN A. BERGIN,³ MARTIN S. HOLDREN,¹ GABI WENZEL,^{1,4} CI XUE,¹ TROY VAN VOORHIS,¹ AND BRETT A. MCGUIRE^{1,5}

¹Department of Chemistry, Massachusetts Institute of Technology, Cambridge, MA 02139, USA

²Department of Chemistry, Virginia Military Institute, Lexington, VA 24450, USA

³Department of Astronomy, University of Michigan, Ann Arbor, MI 48109, USA

⁴Center for Astrophysics | Harvard & Smithsonian, Cambridge, MA 02138, USA

⁵National Radio Astronomy Observatory, Charlottesville, VA 22903, USA

ABSTRACT

Elemental abundances, which are often depleted with respect to the solar values, are important input parameters for kinetic models of interstellar chemistry. In particular, the amount of carbon relative to oxygen is known to have a strong effect on modeled abundances of many species. While previous studies have focused on comparison of modeled and observed abundances to constrain the C/O ratio, the effects of this parameter on the underlying chemistry have not been well-studied. We investigated the role of the C/O ratio on dark cloud chemistry using the NAUTILUS code and machine learning techniques for molecular representation. We find that modeled abundances are quite sensitive to the C/O ratio, especially for carbon-rich species such as carbon chains and polycyclic aromatic hydrocarbons (PAHs). CO and simple ice-phase species are found to be major carbon reservoirs under both oxygen-poor and oxygen-rich conditions. The appearance of C₃H₄ isomers as significant carbon reservoirs, even under oxygen-rich conditions, indicates the efficiency of gas-phase C₃ formation followed by adsorption and grain-surface hydrogenation. Our model is not able to reproduce the observed, gas-phase C/H ratio of TMC-1 CP at the time of best fit with any C/O ratio between 0.1 and 3, suggesting that the modeled freeze-out of carbon-bearing molecules may be too rapid. Future investigations are needed to understand the reactivity of major carbon reservoirs and their conversion to complex organic molecules.

1. INTRODUCTION

Within the context of interstellar chemistry, carbon plays a central role. Carbon comprises the backbone of all organic molecules, many of which are key ingredients for life on Earth. Although a sizable portion of interstellar carbon is thought to exist in atomic/ionic form or as CO depending on the visual extinction of the region, 10-25% is thought to be contained in polycyclic aromatic hydrocarbons (PAHs) (Dwek et al. 1997; Habart et al. 2004; Tielens 2008; Chabot et al. 2019). Additionally, the detections of numerous complex organic molecules within the interstellar medium (ISM) indicate that some portion of carbon is contained within these species (McGuire 2022; Yang et al. 2022; McClure et al. 2023; Salyk et al. 2024; Xue et al. 2025). Many of these complex organic molecules have been detected at the

cyanopolyne peak in the cold and dense Taurus Molecular Cloud 1 (TMC-1 CP), evidencing that complex carbon chemistry can occur even at very low temperatures. In particular, CN-derivatives of naphthalene (McGuire et al. 2021), acenaphthylene (Cernicharo et al. 2024), pyrene (Wenzel et al. 2024a,b) and coronene (Wenzel et al. 2025) have recently been detected in TMC-1 CP. The pure hydrocarbons pyrene and coronene are estimated to each contain approximately 0.04% of the total carbon when accounting for depletion onto dust grains, suggesting that individual PAHs can be significant reservoirs of carbon within cold molecular clouds. This would be a significant component of the interstellar PAH population if this material is returned to the ISM. However, kinetic models built to simulate the chemical evolution of dense clouds have historically failed at reproducing the observed abundances of carbon-containing molecules, particularly larger ones (Byrne et al. 2023).

When investigating the interstellar formation of carbon-bearing molecules, it is first necessary to have an understanding of the elemental abundances available

Corresponding author: Alex N. Byrne, Brett A. McGuire
 lxbyrne@mit.edu, brettmc@mit.edu

within that region. Observations of atomic absorption lines toward various regions of the ISM have found that gas-phase atomic abundances of carbon and heavier elements are depleted with respect to the solar abundances - the elemental abundance ratios in our solar system based on measurements of the Sun's photosphere and carbonaceous meteorites (Morton et al. 1973; Morton 1974; Lodders 2003; Jenkins 2009). This depletion is thought to relate to the presence of these elements as key components of refractory solids or dust grains (Morton 1974). Using gas-phase elemental abundances observed toward 243 sight lines, (Jenkins 2009) derived a relationship between the depletion of a particular element and the overall depletion of a sight line. These depletion factors serve as a baseline for estimating gas-phase elemental abundances of interstellar sources.

Historically, kinetic models of dense clouds have often adopted elemental abundances based on those of the diffuse cloud ζ Oph as it is a well-studied source with observed depletion in many elements (Graedel et al. 1982; Savage et al. 1992; Jenkins 2009). Updated values from the analysis by Jenkins (2009), preferred by many recent studies, result in a C/O ratio of ~ 0.55 (Hincelin et al. 2011; Agúndez & Wakelam 2013). It has long been known that kinetic models of interstellar chemistry are highly sensitive to this parameter, including isotopic fractionation (Langer et al. 1984; Langer & Graedel 1989) as well as the abundances of many carbon-containing species, from atomic carbon to complex organic molecules (Herbst 1983; Langer et al. 1984; Herbst & Leung 1986; Langer & Graedel 1989; Wakelam et al. 2010; Hincelin et al. 2011; Loomis et al. 2021). Although the solar abundance of oxygen is greater than that of carbon by a factor of two (Lodders 2003), multiple mechanisms have been proposed that could modify the gas-phase C/O ratio as a diffuse cloud collapses to a dense cloud. For example, the efficient freeze-out of water onto interstellar grains at low temperatures could deplete oxygen from the gas-phase as the cloud collapses (Furuya et al. 2015; Ruaud et al. 2018). In conjunction with a some mechanism of supplying carbon, such as destruction of carbonaceous grains (Bocchio et al. 2014) or CO (Sellek & Dishoeck 2025), this could lead to enhanced C/O ratios above one at the beginning of the dense cloud phase.

It has been found that a larger C/O ratio than originally used often provides better agreement between kinetic models and observations (Herbst 1983; Watt et al. 1986; Swade 1989; Bergin 1995). Hincelin et al. (2011) studied the effects of a decreasing initial oxygen abundance on a kinetic model of dark cloud chemistry. The authors found that an additional depletion of over a

factor of 2 in oxygen was necessary to produce modeled O_2 abundances in agreement with observations. They also found that this depleted oxygen abundance resulted in better overall agreement between modeled and TMC-1 CP observed abundances, partially due to larger abundances of cyanopolyyynes (HC_nN , $n = \text{odd}$). Likewise, Loomis et al. (2021) performed kinetic modeling of cyanopolyyynes up to HC_{11}N in a dark cloud using a range of oxygen abundances and thus C/O ratios, finding that a ratio of 1.1 provides excellent agreement with TMC-1 CP observations whereas a ratio of 0.7 results in considerably poor agreement. Agúndez & Wakelam (2013) compared the fraction of reproduced molecules for 70 TMC-1 CP abundances using the 2011 KIDA and UMIST RATE12 chemical networks and C/O ratios of 0.55 and 1.4. Contrary to the aforementioned studies, the authors found that the C/O ratio of 0.55 resulted in a greater percent of molecules reproduced by the model, although only these two ratios were considered. Furthermore, the chemical networks used have undergone substantial changes since such as the inclusion of additional complex organic molecules, refinement of reactions and rate coefficients, and incorporation of ice-phase chemistry.

It thus remains unclear which elemental abundances of carbon and oxygen best represent the amounts present in TMC-1 CP, with proposed C/O ratios spanning a large range from 0.55 to 1.4 (Agúndez & Wakelam 2013). Furthermore, while previous analyses have focused on the effect of C/O ratio on agreement with observations, there has been less emphasis on the influence that this parameter has on the underlying chemistry. Such an understanding is vital as the number of detected molecules, including long carbon chains and PAHs, continues to grow. A comprehension of the chemical effects of the C/O ratio is also necessary for generalizing results from TMC-1 CP to other dark clouds or to the following protoplanetary disk stage.

Here we present an analysis on the influence of the C/O ratio on dark cloud chemistry using kinetic modeling and machine learning. In Section 2 we describe the modeling code and parameters used, the modification of the C/O ratio, and the implementation of machine learning embedding to visualize the molecules in the network. In Section 3 we show the sensitivities of carbon-bearing molecules to the C/O ratio, the time-dependent carbon fractions of major carbon reservoirs, and the partitioning of carbon between gas and ice phase as a function of C/O ratio. In Section 4 we discuss the implications of these results for interstellar carbon chemistry. Finally, in Section 5 we summarize the major findings and propose areas for further investigation.

2. METHODS

We use the 2016 version of the **NAUTILUS** 3-phase modeling code, an open-source rate equation code (Ruaud et al. 2016). This code has been extensively used in modeling of molecular clouds such as TMC-1 CP (e.g. Shingledecker et al. 2018; Navarro-Almaida et al. 2020). **NAUTILUS** treats the gas phase, grain surface, and grain mantle as separate phases, each with their own set of chemical reactions. Rates of adsorption onto grain surfaces, desorption from grain surfaces, and swapping between grain surface and mantle are also computed. The considered desorption mechanisms consist of thermal evaporation, evaporation via cosmic-ray heating, photodesorption by external and internal, cosmic-ray induced photons, and chemical desorption due to reaction exothermicity (Garrod et al. 2007). The physical conditions used are those considered typical of a cold dark cloud, consisting of a kinetic temperature of 10 K for the gas and dust grains (Pratap et al. 1997; Fehér et al. 2016; Fuente et al. 2019), a gas number density of $2 \times 10^4 \text{ cm}^{-3}$ (Snell et al. 1982; Fehér et al. 2016; Fuente et al. 2019), a cosmic-ray ionization rate of $1.3 \times 10^{-17} \text{ s}^{-1}$ (Spitzer & Tomasko 1968; Dalgarno 2006; Padovani et al. 2009), and a visual extinction of 10 mag for external UV photons Fuente et al. (2019); Rodríguez-Baras et al. (2021). The initial elemental abundances chosen are those from Byrne et al. (2023). These are primarily the “low-metal” abundances from Graedel et al. (1982). The gas- and ice-phase reactions, hereafter referred to as chemical networks, are those used and described in Byrne et al. (2024). These networks are based on kida.uva.2014 (Wakelam et al. 2012) and Ruaud et al. (2015) respectively and include a number of changes related to recently-detected species such as large carbon chains and aromatic molecules. For example, our network considers formation of cyanonaphthalene ($\text{C}_{10}\text{H}_7\text{CN}$) through reactions involving benzene (C_6H_6) and phenyl radical (C_6H_5), along with multiple pathways to forming six-membered aromatic rings.

To assess the effect of the C/O ratio on model results, 100 equally-spaced values for the C/O ratio over a range of 0.1 to 3.0 were tested as functions of varying initial carbon and oxygen abundances. These variations to the initial C/O ratio can be considered as a simple proxy for some mechanism that modifies the gas-phase elemental abundances as the dense cloud forms, for which a more detailed consideration is beyond the scope of this work. For every C/O ratio, two iterations of the model were performed: one where the ratio was achieved by increasing or decreasing the initial carbon abundance from its nominal value of 1.70×10^{-4} , and one where the ratio was achieved by increasing or decreasing the initial oxygen

abundance from its nominal value of 1.55×10^{-4} . Our nominal oxygen abundance is lower than the ζ Ophiuchi value of Jenkins (2009) as it has been found to better reproduce the TMC-1 CP abundances of cyanopolyyynes (Loomis et al. 2021). For example, to test a C/O ratio of 0.5, we create two models: one with initial carbon and oxygen abundances of 7.75×10^{-5} and 1.55×10^{-4} respectively, and another with initial carbon and oxygen abundances of 1.70×10^{-4} and 3.40×10^{-4} respectively. In this way the initial abundances of carbon and oxygen were never changed concurrently. Time-dependent sensitivities of modeled abundances to C/O ratio were determined by calculating the relative standard deviation of these abundances as a function of C/O ratio at select times. This same metric was found to be a valid measure of sensitivity of modeled abundances to reaction rate coefficients (Byrne et al. 2024). It is widely believed that the “chemical age” of TMC-1 CP lies between 10^5 and 10^6 years based on agreement between kinetic models and observations (Hincelin et al. 2011; Agúndez & Wakelam 2013; Ruaud et al. 2016). Recent modeling studies find the best agreement at a time of $\sim 5 \times 10^5$ years, especially for more complex molecules such as PAHs and cyanopolyyynes (Loomis et al. 2021; Chen et al. 2022; Byrne et al. 2023). For the proceeding analyses we thus focus on a time of 505,500 years, hereafter referred to as 5×10^5 years.

In order to better visualize and analyze the resulting data, we made use of machine learning and data science techniques. We used a pipeline similar to that used in prior machine learning of interstellar chemical inventories and molecular property prediction (Lee 2021; P. Fried et al. 2023; Scolati et al. 2023; Toru Shay et al. 2025; Marimuthu & McGuire 2025). First, a SMILES (Simplified Molecular Input Line Entry System) string is supplied for each carbon-containing species in our chemical network. These strings are a convenient, machine-readable format for writing out chemical structures (Weininger 1988). The SMILES strings are then converted to SELFIES strings, which are a similar representation but more robust and designed specifically for use in machine learning (Krenn et al. 2020). Next, the SELFIES strings are passed through the VIG-GAE embedder where each SELFIES string is converted to a 32-dimensional vector. This is a pretrained, astrochemistry-focused embedding model that captures chemical characteristics of each molecule within the dense, 32-dimensional vectors created. Information regarding properties such as size, connectivity, charge, and degree of saturation is encoded into these vectors, although individual vector dimensions themselves do not map directly to properties. This treatment is particu-

larly useful for comparing the “chemical similarity” of multiple species, as the distance in vector space between two molecules corresponds to their similarity as learned by the VICGAE embedder. In order to visualize this vector space in two dimensions, we finally make use of the UMAP (Uniform Manifold Approximation and Projection; [Sainburg et al. \(2021\)](#)) algorithm to determine a set of two-dimensional vectors that best matches the structure of the 32-dimensional vector space. We use 75 neighbors, the euclidean metric, a minimum distance of 0.1, and a spread of 1 as our UMAP parameters. The end result is a set of two-dimensional vectors for each carbon-containing species that can be plotted to visualize the entire chemical network at once in terms of machine-learned chemical similarity.

3. RESULTS

3.1. *Model sensitivity to C/O ratio*

For each species, the modeled abundances of that species at 5×10^5 years were collected from all models with varying C/O ratios. The relative standard deviation was calculated for each species by determining the standard deviation of these abundances and then dividing by the average. This relative standard deviation metric is a normalized measure of the spread in abundances as a function of C/O ratio. A larger relative standard deviation thus indicates that modeled abundances change more drastically as a function of C/O ratio, leading to a greater spread in the data. In Figure 1 the 10 most sensitive species to the C/O ratio at 5×10^5 years according to this metric are shown for three different ranges of C/O ratios. This data is from the models where only the initial oxygen abundance has been changed, as this is the manner in which the C/O ratio is typically changed. Changing the initial carbon abundance can lead to additional effects as both the amount of carbon relative to oxygen and absolute amount of carbon are changing ([Kanwar et al. 2025](#)). These regimes consist of C/O ranges of 0.1 to 1.0, 0.5 to 2.0, and 2.0 to 3.0. Hereafter the terms “oxygen-rich” and “oxygen-poor” are used to refer generally to models where the C/O ratio is below or above unity respectively as a result of changing the initial oxygen abundance. We note that the range of 0.1 – 1.0 encompasses the entire oxygen-rich range tested, while the range of 2.0 – 3.0 is a specific subset of oxygen-poor conditions that is substantially above unity. This is because there is significantly different effects of changing C/O ratio on modeled abundance at C/O ratios well above unity compared to C/O ratios near unity. The range of 0.5 – 2.0 can roughly be considered an “astrophysically reasonable” range as it encompasses the range of C/O ratios

used in other studies of dense clouds, typically spanning from 0.5 to 1.4 ([Agúndez & Wakelam 2013](#); [Chen et al. 2022](#)). While C/O ratios approaching 2.0 are larger than those typically used for dense clouds, they are consistent with models and observations of protoplanetary disks ([Bergin et al. 2016](#); [Kanwar et al. 2024](#); [Sellek & Dishoeck 2025](#)).

The C/O = 0.1 – 1.0 regime is characterized by large relative standard deviations for two main classes of molecules. The first is small, oxygen-bearing molecules such as OCN and H₂CN in the ice phase. The abundances of these species quickly drop as the C/O ratio rises due to oxygen depletion. The second is long, unsaturated carbon-chain species with 9–11 carbon atoms in the gas phase. As the window of C/O ratios shifts toward greater values, the overall relative standard deviations decrease and the identities of the most sensitive species change. In the C/O = 0.5 – 2.0 range, the greatest relative standard deviations are now ~ 1.6 for the two-ring PAH naphthalene (C₁₀H₈) and the hydronaphthalenes (C₁₀H₁₀, C₁₀H₉, both in the gas phase and in the ice). These bicyclic PAHs are the only PAHs currently included in the model; larger PAHs whose cyano derivatives have been detected, specifically pyrene, coronene, and acenaphthylene, have not yet been added. When the C/O ratio is increased above 2.0, these species remain the most affected although the relative standard deviations are much lower at ~ 0.5 . A few ice-phase, oxygen-bearing molecules, specifically CO₂, CH₃CO, CH₃OCH₃ also appear here. The sharp decrease to relative standard deviations as the C/O ratio increases shows that modeled abundances are less sensitive to a changing oxygen abundance as oxygen becomes more depleted from the gas phase. It is under oxygen-rich conditions where changing the initial oxygen abundance has the strongest impact on modeled abundances. Recently we performed a sensitivity analysis of an astrochemical model to the rate coefficients of gas-phase reactions ([Byrne et al. 2024](#)). We found that the greatest sensitivity of a species abundance to an individual rate coefficient was a relative standard deviation of 1.43. Overall, abundances in our model are substantially more sensitive to the C/O ratio than any individual rate coefficient, especially within the regime of 0.1 – 1.0.

The modeled abundances with respect to hydrogen nuclei of C₁₁ and C₁₀H₈ as a function of time for all tested C/O ratios are shown in Figures 2 and 3, again with models where only the initial oxygen abundance was modified. In addition to the minimum and maximum C/O ratios tested, the abundance profile resulting from our “nominal” C/O ratio of 1.1 is shown in orange. This value, obtained by lowering the initial oxygen abundance

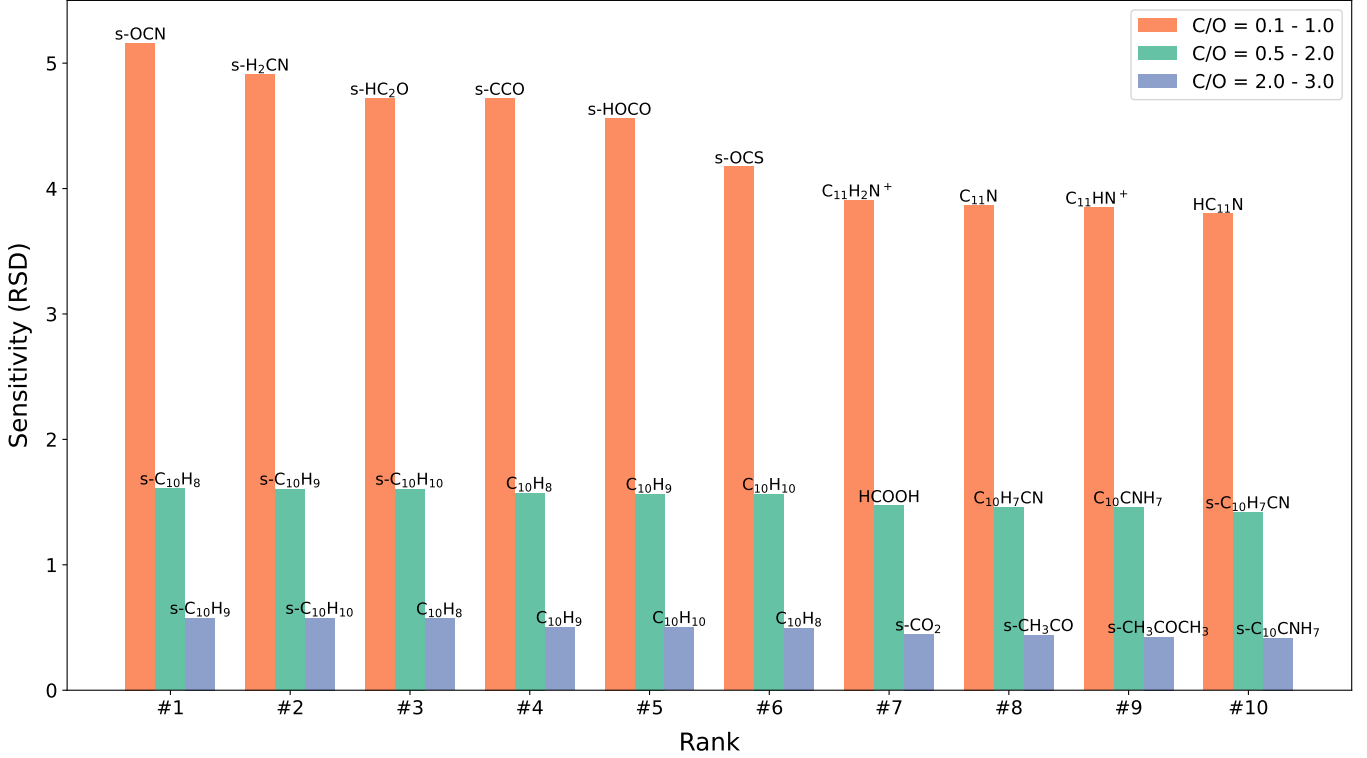


Figure 1. Top 10 most sensitive carbon-containing species to the C/O ratio at 5×10^5 years according to relative standard deviation. Relative standard deviations are shown for three different ranges of C/O ratio as discussed in the text: C/O = 0.1–1.0 (orange), C/O = 0.5–2.0 (green), and C/O = 2.0–3.0 (blue). Each bar is annotated with the formula of the corresponding species as it appears in the model. Species names with a prefix of “s-” correspond to ice-phase species where the abundances in the surface and mantle phases have been summed together

, while the absence of a prefix indicates a gas-phase species.

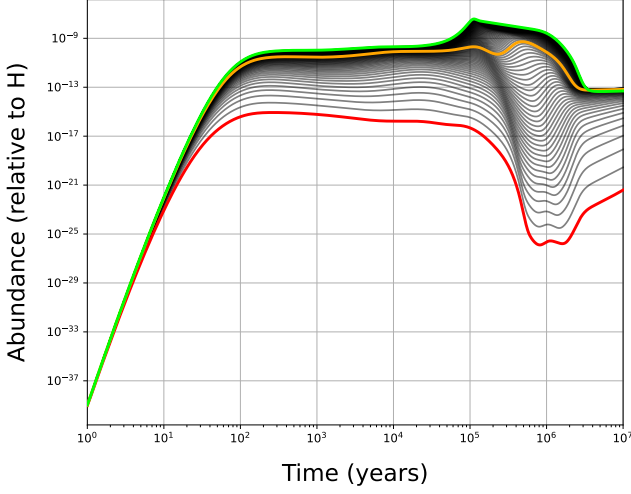


Figure 2. Modeled abundances relative to H of C₁₁ as a function of time for every tested C/O ratio. The minimum ratio of 0.1 is shown in red, the nominal ratio of 1.1 is shown in orange, and the maximum ratio of 3.0 is shown in green.

to 1.55×10^{-4} , has been found by Loomis et al. (2021) to well reproduce the abundance of cyanopolyyynes and

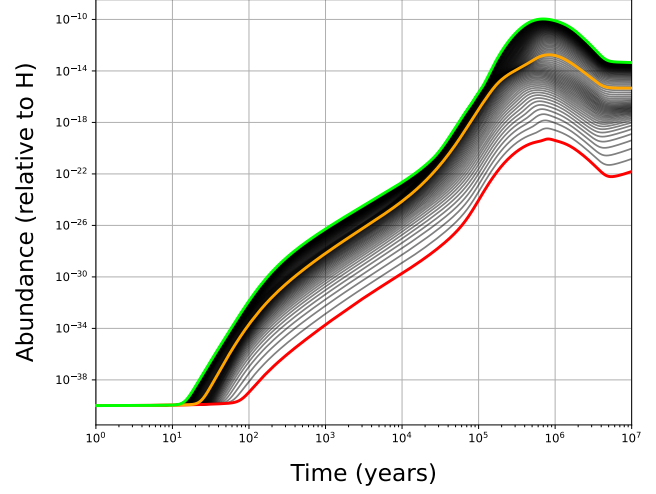


Figure 3. Same as Figure 2 but for C₁₀H₈.

is the typical value used in our model. Between 10^5 and 10^6 years the abundance of C₁₁ drops substantially in models where the C/O ratio is low, with almost a 15 order of magnitude difference between the nominal and lowest abundances. Conversely, the abundance of C₁₀H₈

does not show a marked change in abundance profile but rather diminished production, with a ~ 7 order of magnitude difference in nominal and minimum abundance in the aforementioned time range. Increasing the C/O ratio shows diminishing returns in terms of abundance increases in both species. For C₁₁, the abundance at 5×10^5 years is only about an order of magnitude larger in the model with a C/O ratio of 3 compared to the nominal model. Conversely, the abundance of C₁₀H₈ increases by a little over three orders of magnitude under the same circumstances. The diminishing changes to abundances, such as those of C₁₁ and C₁₀H₈, as the C/O ratio is increased up to 3.0 is why the relative standard deviations are significantly lower in the C/O = 2.0-3.0 regime.

3.2. Carbon Reservoirs and carbon chemistry

In Figures 4, 5, and 6 the modeled time-evolution of fraction of carbon in all carbon-containing species is shown for models with oxygen-rich conditions ($C/O = 0.5$), equal carbon and oxygen ($C/O = 1$), and oxygen-poor conditions ($C/O = 2.0$) respectively. As in Section 3.1, we use the models where only initial oxygen abundance is changed to focus on C/O ratio as a function of oxygen depletion. These figures display every carbon-containing molecule in our network plotted as its UMAP dimensions obtained from the procedure described in Section 2. As mentioned previously, the values of these UMAP dimensions do not directly convey any molecular information. Instead, they represent a molecule’s position in a machine-learned vector space based on properties such as size, and connectivity. In this way, a large number of molecules can be visualized concurrently with the distances between them proportional to their chemical similarities as learned by the VICGAE embedder, which may differ from human intuition. Each dot in these figures corresponds to one molecule, while the size of the dot is proportional to the fraction of total carbon contained in this molecule at the displayed time. The color of the dot corresponds to the elemental composition, namely the presence of heteroatoms or aromaticity. For molecules containing multiple heteroatoms or containing a heteroatom and aromaticity, aromaticity takes highest priority for the color coding, followed by the presence of silicon, sulfur, oxygen, and nitrogen. There are no carbon-containing species in the model that have a phosphorus, fluorine, or chlorine atom and are aromatic or contain another heteroatom.

Starting at approximately 1000 years, the primary form of carbon begins shifting from gas-phase atomic form to simple gas- and ice-phase species. Between

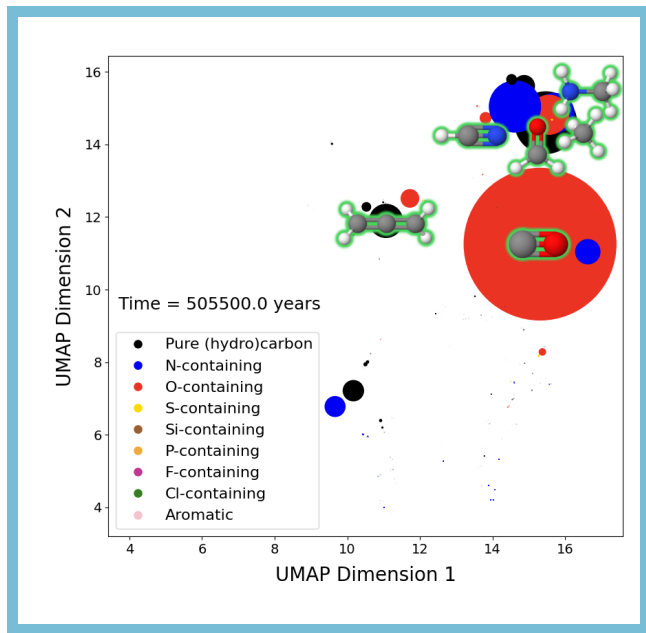


Figure 4. Modeled time-dependent carbon fractions of every carbon-containing species in the network with a C/O ratio of 0.5. Each dot represents a species that contains carbon plotted according to its UMAP vectors. The color corresponds to the elemental composition, while the size is the fraction of carbon multiplied by a scaling factor. Molecular structures are shown for species comprising at least 2% of the total carbon. Some of structures are slightly offset from their corresponding dots for visual clarity. Structures for ice-phase (grain surface or mantle) species are highlighted in green. At the beginning of the simulation, nearly all of the carbon is in atomic form as represented by a large black dot in the center-right of the figure. Starting at ~ 100 years, a red dot slightly to the left of atomic carbon corresponding to CO begins to grow. At 500 years, a handful of dots clustered near the upper right corner also begin to slowly grow. These correspond to ice-phase HCN, H₂CO, CH₄, and CH₃NH₂. These species continue to grow in carbon fraction as time progresses, with CO reaching the 2% of total carbon threshold at 4695 years. Starting at 10^4 years, the dot corresponding to atomic carbon begins to rapidly diminish while the aforementioned dots grow more rapidly. A black dot below CO corresponding to C₃ quickly grows from this point, reaching the 2% threshold at 11220 years. At 19420 years ice-phase CO also reaches the 2% threshold. At 3×10^4 years ice-phase H₂CO reaches 2% of the total carbon budget, followed shortly by HCN, CH₃NH₂, and CH₄ all in the ice phase as well. At 10^5 years atomic carbon begins to rapidly shrink in abundance, followed shortly by C₃. Gas-phase CO peaks in size at $\sim 2 \times 10^5$ years and then decreases whereas ice-phase CO rapidly expands. There are also a few dots representing pure hydrocarbons, oxygen-containing species, and nitrogen-containing species that become sizable in terms of carbon fraction. The only one of these that reaches the 2% threshold is ice-phase CH₂CCH₂ at 3.54×10^5 , located a bit to the left of CO and growing in size until $\sim 10^6$ years. Between 10^6 years and the end of the simulation at 10^7 years there are few changes except a decline in CH₃NH₂, the appearance of ice-phase HNC as significant carbon reservoir near CO and atomic carbon, and continued growth of ice-phase CH₄. The static image displays the major reservoirs of carbon (those containing at least 2% of the total carbon) at $\sim 5 \times 10^5$ years, where our model best reproduces the abundances of larger carbon-bearing molecules.

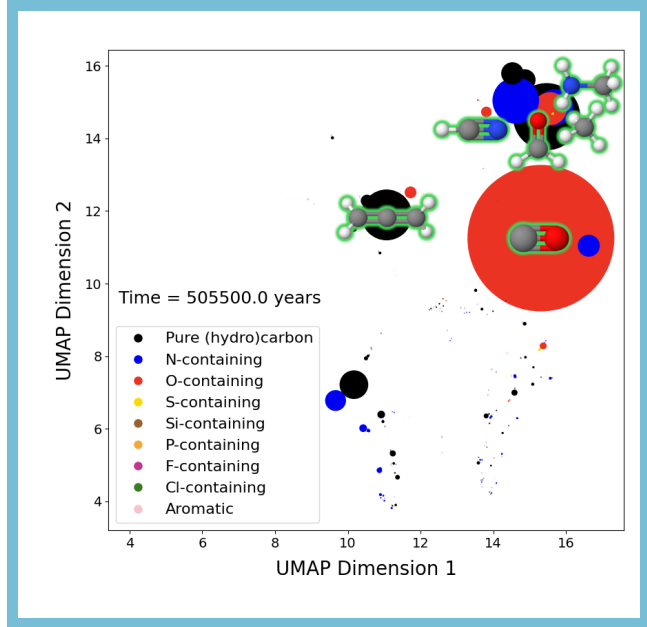


Figure 5. Same as Figure 4 but with a C/O ratio of 1. The evolution of carbon fractions begins very similarly to that of a C/O ratio of 0.5, although CO forms more slowly and does not reach the 2% threshold until 5698 years. C_3 reaches this same threshold immediately after at a time of 5791 years. As in Figure 4, atomic carbon begins to quickly diminish at 10^4 years whereas C_3 , CO, ice-phase CO, and ice-phase HCN, H_2CO , CH_4 , and CH_3NH_2 grow in size more quickly. Ice-phase CO achieves a carbon fraction of 2% at 26390 years, followed by HCN, H_2CO , CH_4 , and CH_3NH_2 at $\sim 4 \times 10^4$ years. By 10^5 years C_3 is the second largest carbon reservoir next to CO, almost triple the size as in the model with a C/O of 0.5 at this time. Following this time there is rapid gain of ice-phase CO and loss of atomic carbon and C_3 followed by gas-phase CO, although C_3 maintains a carbon fraction of at least 2% until a time of 3.78×10^5 years compared to 3.02×10^5 years in Figure 4. A growth in various nitrogen-containing, oxygen-containing, and pure hydrocarbon species is again seen although at an earlier time and to a stronger extent. CH_2CCH_2 reaches the 2% threshold at 1.58×10^5 years followed by its isomer CH_3CCH at 1.83×10^5 years. The dot for CH_3CCH is located a good distance below that of CH_2CCH_2 at the top of a series of dots that extends down to the bottom of the graph. Between 10^5 and $\sim 5 \times 10^5$ many dots in this series, along with another series on the right side of the figure below CO, grow in size sequentially, although none of them reach a carbon fraction of 2%. The carbon fraction of CH_3CCH diminishes from 3×10^3 years and drops below 2% by 4.37×10^5 years, while the fraction of carbon in CH_2CCH_2 continues to grow. Between 10^5 years there is also a decline in ice-phase CH_3NH_2 and a growth in ice-phase CH_4 . From 10^6 to 10^7 years the major observations are the appearance of ice-phase C_3H_8 as a major carbon reservoir at 10^6 years in the top-right cluster, a continued growth in ice-phase CH_4 , and the continued diminishing of various other species such as the series of dots that extend toward the bottom of the figure.

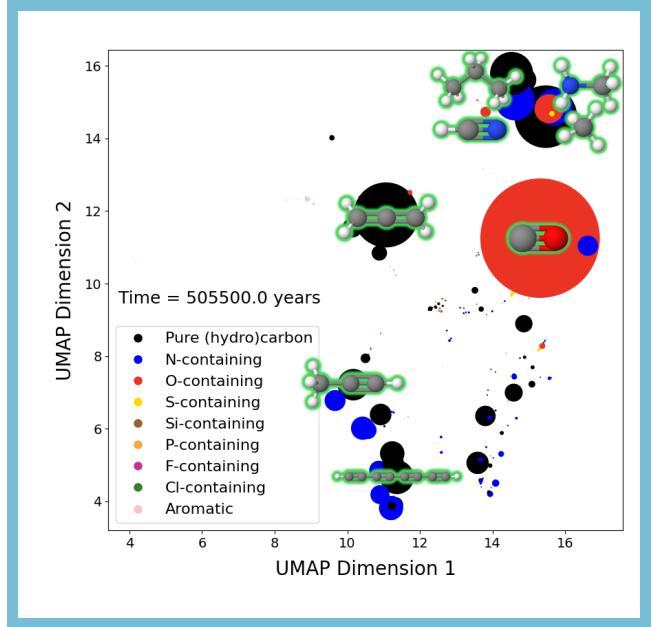


Figure 6. Same as Figures 4 and 5 but with a C/O ratio of 2.0. Compared to the previous figures there is an even faster growth of C_3 here, with it reaching the 2% threshold at 3869 years even before CO at 5607 years. Between 10^4 and 10^5 years the carbon fraction of atomic carbon again decreases while the fractions in CO and C_3 grow. The sizes of CO and C_3 are almost equal over this range of time. Again ice-phase CH_3NH_2 , CH_4 , H_2CO , and HCN become major carbon reservoirs, although here CH_3NH_2 is the first to reach 2% at $\sim 3 \times 10^4$ years. This is followed shortly by CH_4 at $\sim 4 \times 10^4$ years, and then HCN and H_2CO at $\sim 8 \times 10^4$ years. Over this range of 10^4 to 10^5 years there can also be seen the growth of nitrogen-containing and pure hydrocarbon species near CH_2CCH_2 and CH_3CCH . Following 10^5 years the carbon fractions in gas-phase CO and C_3 again diminish as ice-phase CO grows, however there are a number of differences compared to the previous figures. The sequential growth in the nitrogen-containing and pure hydrocarbon species below CH_3CCH and below CO is much more pronounced. At 3.32×10^5 years, one of these dots corresponding to C_8H_2 reaches 2% of the total carbon, although a number of nearby dots appear to be only slightly smaller in size. These species again diminish in size following 5×10^5 years, except for ice-phase C_8H_3 which appears at $sim 9 \times 10^5$ years and remains until the end of the simulation. In the top-right corner ice-phase H_2CO drops below 2% of all carbon shortly after 10^5 years but returns at 8×10^5 years, while ice-phase C_3H_8 reaches 2% at 2.45×10^5 years. From 10^6 until 10^7 years, ice-phase CH_2CCH_2 and CH_4 continue to grow in size. A few new species additionally appear as major carbon reservoirs. Ice-phase CH_2CHCCH appears near CH_2CCH_2 shortly after 10^6 years, followed quickly by ice-phase C_2H_6 near CH_4 and C_3H_8 . Finally, C_6H_4 located below CO becomes a major reservoir of carbon at 1.35×10^6 years.

$\sim 5 \times 10^4$ and 10^5 years, these major reservoirs of carbon are gaseous C, CO, and C₃, which are clustered in the middle-right of Figures 4-6, and grain-mantle CH₄, H₂CO, HCN, and CH₃NH₂, which are clustered together in the upper-right. This is the same in both the oxygen-rich (Figure 4) and oxygen-poor (Figure 6) models, although there are small differences in time evolutions of these carbon fractions. In particular, the conversion of atomic carbon to C₃ is significantly faster in the oxygen-poor model as evidenced by the more rapid disappearance of the dot corresponding to atomic carbon and more rapid growth of the dot corresponding to C₃. Starting from 10^5 years, there are drastic and rapid changes to the form of carbon. The amount of carbon in atomic form and gas-phase C₃ quickly drops, while the abundance of ice-phase CO grows as it freezes out from the gas phase. The carbon fractions of grain-mantle CH₄, HCN, H₂CO, and CH₃NH₂ stay relatively constant between 10^5 and 10^6 years with some slight increases and decreases.

Aside from these changes the oxygen-rich and oxygen-poor models diverge significantly. In the oxygen-poor model, there are numerous dots in the bottom half of the figure that quickly grow in size over the range of 10^5 to $\sim 5 \times 10^5$ years. These represent various unsaturated carbon-chain molecules such as C₈H₂, which constitutes slightly more than 2% of the total carbon near the end of this range. Furthermore a sizeable fraction of total carbon is present in the two isomers of C₃H₄, allene (CH₂CCH₂) and propyne (CH₃CCH), in the grain mantle. CH₂CCH₂ can be seen as a major carbon reservoir even in the oxygen-rich model, however this becomes much more pronounced in the oxygen-poor model. By 10^6 years grain-mantle CH₂CCH₂ is the second largest reservoir of carbon at slightly more than 10%. The hydrocarbons C₂H₆, C₃H₈, CH₂CHCCH, C₆H₄, and C₈H₄ in the grain mantle additionally become significant carbon reservoirs in the oxygen-poor model as the simulation progresses to 10^7 years. The model with a C/O ratio of 1 (Figure 5) is an intermediate between the oxygen-rich and oxygen poor scenarios. Even in this model the faster conversion of atomic carbon to C₃ and appearance of gas-phase carbon chains can be seen, although not to the degree of the oxygen-poor model. The time-dependent carbon reservoirs in our model are thus highly dependent on C/O ratio with gas-phase carbon chains and grain-mantle hydrocarbons becoming more abundant as the C/O ratio increases.

3.3. Fractions of carbon in the gas and grain phases and comparison with observations

Recently Xue et al. (2025) have compiled and re-analyzed the column densities of many of the detected TMC-1 CP species to-date. The authors converted these column densities to abundances of carbon with respect to hydrogen nuclei, finding a total gas-phase carbon abundance of 5.0×10^{-5} when summed together. Many chemical kinetic models of TMC-1 CP assume a total carbon budget of 1.7×10^{-4} with respect to hydrogen nuclei based on observations of the diffuse cloud ζ Ophiuchi (Jenkins 2009; Agúndez & Wakelam 2013). The observed value from Xue et al. (2025) is 29.4% of this, suggesting that the detected, gas-phase molecular inventory of TMC-1 CP accounts for approximately 30% of the total carbon budget if the ζ Ophiuchi value is indeed representative. We note that this observation-based value does not consider uncertainties in the column densities. Although individual column densities are often well-constrained, there is a currently unquantified uncertainty in this gas-phase carbon budget due to the combination of these observational uncertainties. In Figure 7 we compare the observed gas-phase carbon fraction from Xue et al. (2025) with the gas- and ice-phase carbon fractions as obtained by our model. We plot the modeled fractions as a function of C/O ratio for both changing initial oxygen and carbon abundances and for simulation times of 1×10^5 , 3×10^5 , and 5×10^5 . In each plot we show the value from Xue et al. (2025) as a horizontal black dashed line.

In all cases the gas-phase carbon fraction increases with increasing C/O ratio, although this is relatively small with a maximum difference of $\sim 10\%$ over the entire range tested. At 1×10^5 years, approximately 70% of the total carbon is in the gas-phase for all C/O ratios tested. The amount of gas-phase carbon quickly decreases as time goes on, dropping to 40% at 3×10^5 years and only 20% at 5×10^5 years. The observed value does not include every species that has been detected in TMC-1 CP. More importantly, it does not include a number of carbon-containing species that have not been detected but are known or thought to be present, such as CH₃, C₃, and even atomic carbon itself. These latter two species in particular are highly abundant forms of carbon that are included in our model along with a number of undetected carbon-containing species. We thus expect the observed value from Xue et al. (2025) to underestimate the gas-phase carbon fraction compared to the model. This is true at 1×10^5 and 3×10^5 where the modeled gas-phase carbon fraction is well above and slightly above the observed value respectively, but not

at 5×10^5 years where the model is slightly below the observations.

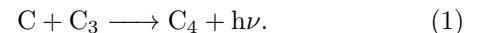
4. DISCUSSION

4.1. Effects of C/O Ratio on Carbon Chemistry

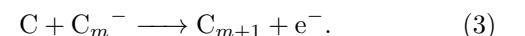
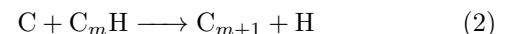
As noted previously, the major carbon reservoirs are relatively insensitive across the range of astrophysically-relevant C/O ratios (between 0.5 and 2.0) and primarily consist of gas-phase C, CO, and C₃ as well as grain-mantle CO, HCN, CH₃NH₂, CH₄, and H₂CO. Aside from CO, which can also be efficiently produced in the gas phase, these species are all formed predominately on the grain surface beginning with atomic carbon. The major formation pathways as identified based on modeled reactions fluxes can be seen in Figure 8. After adsorbing to a grain, atomic carbon can quickly react with other major grain-surface species. At early times these are primarily H, H₂, N, and O. An initial reaction with O or N leads to CO and CN respectively, the latter of which undergoes hydrogenation to HCN via H₂. This is consistent with Ruaud et al. (2016), who likewise found a large abundance of ice-phase HCN in their gas-grain model due to the H₂ + CN reaction when competition between reaction and diffusion is considered. HCN can also be efficiently formed in the gas phase, although its adsorption to grains competes with faster ion-neutral destruction mechanisms (Loison et al. 2014a). Successive hydrogenation of atomic carbon leads to CH₄, although reaction of CH and CH₂ with N and O are competing processes. Addition of O either forms HCO, which is hydrogenated to H₂CO, or H₂CO directly. Addition of N to CH and CH₂ form HCN and H₂CN respectively. The latter is then fully hydrogenated up to CH₃NH₂ by successive additions of atomic hydrogen. Reactions involving atomic hydrogen are generally the fastest grain-surface processes due to its high mobility; however, reactions with O and N are competitive in our model because of their low assumed binding energies of 800 K, compared to 650 K for H. This 800 K value originates from Tielens & Hagen (1982) where it was estimated for C, N, and O. The binding energy of C has since been updated to 4000 K in the model we use (Ruaud et al. 2015), whereas the binding energies of N and O remain at 800 K. More recent computational and experimental work has indicated that the binding energy of O is closer to 1600 K (He et al. 2015; Minissale et al. 2016a; Wakelam et al. 2017; Shimonishi et al. 2018; Minissale et al. 2022), although the binding energy of N has been found to be near or even lower than this original estimate (Minissale et al. 2016a; Wakelam et al. 2017; Shimonishi et al. 2018; Minissale et al. 2022). It has also been suggested more recently that C undergoes chemisorp-

tion rather than physisorption, resulting in even higher binding energies of 10,000+ K (Wakelam et al. 2017; Shimonishi et al. 2018; Minissale et al. 2022). Due to the difficulty in many astrochemical kinetic models assume that the diffusion barriers are related to the binding energies by some universal, constant factor. At a C/O ratio of 2, grain-surface hydrogenation of atomic carbon to CH₄ becomes more efficient because there is less competition from reactions with atomic nitrogen and oxygen. This is likely because the increased amount of reactive, gas-phase carbon at larger C/O ratios leads to more participation of nitrogen and oxygen in gas-phase chemistry at early times and less adsorption onto grain surfaces.

Although these major reservoirs of carbon do not change significantly with varying C/O ratio, there are a number of other noticeable changes. The faster disappearance of atomic carbon as it is converted to carbon-containing molecules, increased abundance of C₃, and decreased abundance of CO with increasing C/O ratio are all signs of enhanced carbon chemistry. This is in line with previous studies (Leung et al. 1984; Blake et al. 1987; Wakelam et al. 2009; Hincelin et al. 2011; Agúndez & Wakelam 2013), as more available carbon relative to oxygen results in more carbon that is not “locked up” in CO and thus able to participate in carbon chemistry. The most striking change is that at C/O ratios above unity, a large number of unsaturated carbon-chain molecules quickly become sizable reservoirs of carbon. These carbon-chain species are sequentially built up via additions of atomic carbon, beginning with the reaction:



Although this is a radiative association mechanism between two small species, previous Rice-Ramsperger-Kessel-Markus (RRKM) calculations suggest a rate coefficient on the order of 10^{-12} at 10 K (Wakelam et al. 2009). Sensitivity analyses of TMC-1 CP kinetic models confirm that this reaction plays a significant role in the network (Wakelam et al. 2009; Byrne et al. 2024). As shown in Figure 9 based on modeled reaction fluxes, formation of C₃ requires two additions of atomic carbon and competes with addition of atomic oxygen to form CO. Formation of larger carbon chains occurs primarily through the reactions



In addition to requiring repeated additions of atomic carbon, all C_mH and C_m⁻ species are quickly destroyed via reaction with atomic oxygen in the model, along with

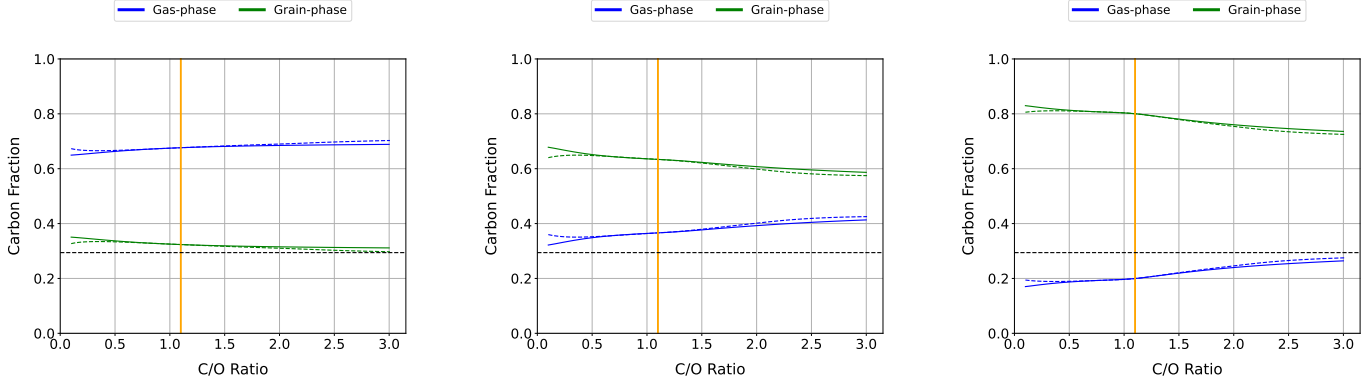


Figure 7. Modeled fractions of total carbon on the grains (green lines) and in the gas-phase (blue lines) at 1×10^5 (left), 3×10^5 (center), and 5×10^5 (right) years. The solid lines are from changing only the initial oxygen abundance, and the dashed lines are from changing only the initial carbon abundance. The black dashed line is the gas-phase carbon fraction based on the observed C/H from Xue et al. (2025) a total carbon abundance of 1.7×10^{-4} . A vertical orange line is plotted at our nominal C/O ratio of 1.1.

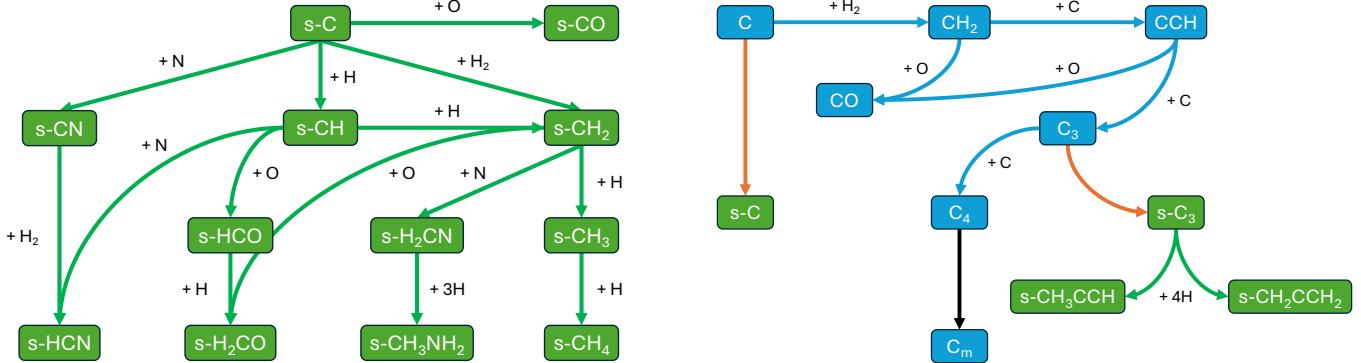


Figure 8. Chemical network leading to the formation of key ice-phase species in our model, beginning with atomic carbon. Each green arrow is a grain-surface reaction, with the other reactant labeled in black. The “s-” prefix denotes grain-surface species.

C_m species with even-numbered m (Loison et al. 2014b). It therefore stands to reason that at low C/O ratios, where there is little carbon available relative to oxygen, these mechanisms will be inefficient. Conversely, the sudden appearance of various carbon-chain species at C/O ratios above one shows that these pathways are considerably important when the amount of available carbon outweighs that of oxygen. This is further confirmed by looking at the contributions of all reactions to the destruction of these species. At a C/O ratio of 0.5, this mechanism is the first or second most influential destruction reaction and accounts of $\sim 20 - 40\%$ of the destruction. When the initial oxygen abundance is depleted to a C/O ratio of 2, it instead accounts for 5% or less of the destruction at later times and is outpaced by reactions with atomic nitrogen, atomic carbon, and small ions such as H_3^+ and HCO^+ .

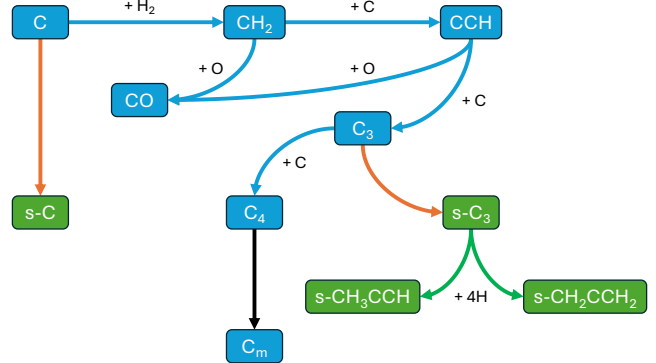


Figure 9. Chemical network leading to the formation of C_3 and beyond in our model. Blue boxes and arrows denote gas-phase species and reactions respectively, while grain-surface species and reactions are in green. Grain-surface species are also labeled with the “s-” prefix. Orange arrows correspond to adsorption to grain surfaces. The black arrow represents carbon-chain growth according to Reactions 2 and 3.

The identification of ice-phase allene (CH_2CCH_2) and propyne (CH_3CCH) as species that contain a significant fraction of total carbon, even at low C/O ratios, is surprising. These two C_3H_4 isomers are pure hydrocarbons, the former of which has no permanent dipole moment and the latter of which has been detected in multiple interstellar regions including TMC-1 CP (Kuiper et al. 1984). Previous modeling work centered on these species has focused on their gas-phase chemistry (Byrne et al. 2023) but did account for grain-surface formation via sequential hydrogenation of C_3 as indicated by Hickson et al. (2016) and Loison et al. (2017). These first four additions of atomic hydrogen are barrierless, however the subsequent hydrogenations to C_3H_5 are expected to have a sizable activation barriers based on the corresponding gas-phase reactions. These barriers in con-

junction with efficient formation of gas-phase C_3 even at low C/O ratios are thus likely why ice-phase CH_2CCH_2 and CH_3CCH are able to build up in large abundance in the model. Between the two, the amount of carbon present in CH_2CCH_2 is two or more times that of CH_3CCH , reaching a staggering 10% of total carbon at large C/O ratios. This is likely due to incomplete inclusion of CH_2CCH_2 into the chemical network. There are numerous ice-phase reactions of CH_3CCH that are missing for CH_2CCH_2 , including hydrogenation to C_3H_5 and beyond. Even so, the presence of these species as major carbon reservoirs is further evidence to the important of C_3H_n hydrocarbons in cold cloud chemistry, for which a major formation route is grain-surface hydrogenation starting from C_3 .

Despite being the most affected molecules when the C/O ratio is varied from 0.5 to 2, naphthalene and related species are not major reservoirs of carbon. Even with a C/O ratio of 2, the maximum carbon fraction obtained by naphthalene is $\sim 1.5 \times 10^{-4}\%$. This is far below the estimated carbon fraction of 0.04% for pyrene and coronene based on observations of the corresponding CN-substituted species (Wenzel et al. 2024a,b, 2025). Although increasing the C/O ratio does provide nonlinear increases to the abundance of $C_{10}H_8$, it alone is not enough to reproduce the abundance of PAHs that are observed in TMC-1 CP. Thus there are important chemical processes that are unaccounted for in the model that convert a significant amount of carbon into these species. In particular, C_3H_n hydrocarbons are precursors to more complex species like benzene (C_6H_6) and naphthalene ($C_{10}H_8$) (Byrne et al. 2023). These species can clearly form in large abundance on grain surfaces in the model. Future work should investigate additional grain-surface reactivity of C_3H_n species as well as their desorption mechanisms.

4.2. Partitioning of Carbon into Gas and Grain Phases

As mentioned in Section 3.3, the approximate gas-phase C/H ratio of TMC-1 CP based on observations cannot be reproduced by the model at 5×10^5 years, even under extreme oxygen-poor conditions. The rapid decrease in the modeled gas-phase carbon fraction over this period of time is due to the freeze out of gaseous molecules, primarily CO, onto grain surfaces. The much larger gas-phase carbon fractions at earlier times of 1×10^5 and 3×10^5 years could suggest that there has been less time for freeze out of gas-phase molecules onto interstellar dust grains in clouds like TMC-1 CP, resulting in lower chemical ages. Additionally, the modeled abundance of gaseous CO, the most abundant carbon-containing molecule, agrees best with observations at an

“intermediate” time of 3×10^5 years. However, it has been shown that the abundances of numerous complex organic molecules such as cyanopolyynes and aromatic species cannot be reproduced until later times closer to 5×10^5 years (Loomis et al. 2021; Byrne et al. 2023). Thus there is a discrepancy between the times at which a substantial fraction of carbon is in the gas-phase and the times at which the modeled kinetics can reach a greater degree of chemical complexity.

One possible solution is that the freeze-out of carbon-containing molecules from the gas phase onto grain surfaces is overly efficient in the model. As shown by the large carbon fractions of ice-phase CH_2CCH_2 and CH_3CCH , large abundances of carbon-containing molecules, including precursors to PAHs and other COMs, can build up on interstellar grains by later times in the model. Grain-surface reactions in the chemical network primarily consist of hydrogenation via hydrogen atoms due to its fast diffusion at 10 K. Carbon atoms have also been shown experimentally to quickly diffuse on low temperature amorphous solid water, although this does not occur until 22 K and above (Tsuge et al. 2023). For grain-surface processes to contribute to the gas-phase chemical inventory, there must be efficient desorption. Thermal evaporation and photodesorption via external UV photons are slow in molecular clouds due to the low temperatures and large densities. Consequently photodesorption via the internal UV field, reactive desorption due to reaction exothermicity, and occasionally cosmic-ray heating of grains are the major processes, with the efficiency of reactive desorption assumed to be 1% (Garrod et al. 2007). This 1% efficiency is the lower-end of the estimated 0.01 – 0.1 range often used in kinetic models. In actuality, this parameter varies from reaction to reaction and is difficult to quantify experimentally (Minissale et al. 2016b; Chuang et al. 2018). Desorption via cosmic-ray sputtering and grain-grain collisions have also been tested in astrochemical models (Wakelam et al. 2021; Kalvāns & Silsbee 2022; Wakelam et al. 2024; Rosandi et al. 2024). These mechanisms are both capable of increasing modeled gas-phase abundances of COMs by multiple orders of magnitude under dense conditions. Further benchmarking of these processes in kinetic models with complex chemistry is necessary.

Another possibility is that there are additional sources of reactive, gas-phase carbon that are not presently considered in the model. As shown in the rightmost panel of Figure 7, we find that increasing the C/O ratio up to 3.0 by increasing the initial carbon abundance still cannot reach a gas-phase carbon fraction of 30%. However, in these scenarios the total carbon budget is greater, and

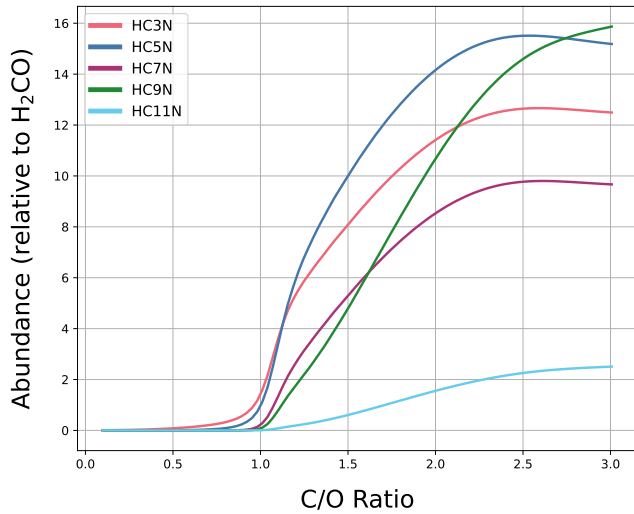


Figure 10. Abundance ratios of detected cyanopolyne species to H_2CO at 5×10^5 years as a function of C/O ratio. Each color represents a different cyanopolyne.

thus the absolute amount of carbon in the gas phase is able to increase above the value determined by (Xue et al. 2025). Such an increase could potentially be achieved by destruction of carbonaceous grains or even large PAHs if the top-down mechanism is operative, although a $\sim 1.36x$ increase to the total carbon budget is required at minimum. In a recent sensitivity analysis (Byrne et al. 2024), we found that many carbon-containing molecules in the model are highly sensitive to the rate of reaction between atomic nitrogen and CN. This is likely because this process frees up atomic carbon from CN that is subsequently used up to form more complex carbon molecules. More processes like this could be responsible for transforming relatively inert forms of carbon species to reactive building blocks, possibly shortening the timescale of formation for PAHs and other COMs. In particular the main reservoir of carbon is in CO; however the only major processes known to break apart CO in molecular clouds are cosmic ray dissociation and ion-neutral reaction with He^+ . These explanations thus seem less plausible than uncertainties in grain-surface processes.

4.3. Astrochemical Implications

According to the sensitivities shown in Figure 1, unsaturated, carbon-rich molecules such as polyynes and PAHs are some of the most sensitive species to the modeled C/O ratio. Similarly, Burkhardt et al. (2021) compared observed abundances of HC_9N and $\text{C}_6\text{H}_5\text{CN}$ across various sources, finding that the abundance ratios of HC_7N and HC_9N to benzonitrile are up to five times larger in TMC-1 CP compared to sources in the

Serpens cloud. Using astrochemical modeling the authors also showed that the cyanopolynes more drastically decrease in abundance as the C/O ratio is lowered compared to $\text{C}_6\text{H}_5\text{CN}$. The large abundance of cyanopolynes relative to $\text{C}_6\text{H}_5\text{CN}$ could thus be evidence of TMC-1 CP having a C/O ratio above unity. It has previously been suggested that abundance gradients within the Taurus Molecular Cloud are due to a variation in C/O ratio, with a greater C/O ratio at the cyanopolyne peak (Pratap et al. 1997). Our findings are also consistent with the idea that a C/O ratio above 1 better reproduces the abundances of complex hydrocarbons observed toward this position (Wakelam et al. 2006; Loomis et al. 2021; Burkhardt et al. 2021). However, other recent modeling studies have indicated that a lower C/O ratio of 0.5-0.7 can provide better agreement with observations (Agúndez & Wakelam 2013; Loison et al. 2014b; Chen et al. 2022). Agúndez & Wakelam (2013) and Chen et al. (2022) both found that a diffuse cloud C/O ratio of ~ 0.5 best reproduces observed abundances in TMC-1 CP. The authors of both studies attribute this to the overproduction of large carbon chains, such as C_nH^- and C_nH_2 species, between 10^5 and 10^6 years when the C/O ratio is above one. As mentioned by Chen et al. (2022), this may be due to a lack of sufficient destruction mechanisms for these large, unsaturated hydrocarbons. However, their best-fit model of uses an elemental carbon abundance of 2.5×10^4 with respect to H nuclei, which is larger than the value of $\sim 1.7 \times 10^4$ typically used. Additionally, the chemical networks used in these studies did not include recently detected COMs such as aromatic species that are highly sensitive to the C/O ratio. PAHs have been proposed to be formed through two major scenarios: “bottom-up” chemistry forming these molecules from smaller precursors, or “top-down” destruction of larger PAHs and carbonaceous dust such as through photodissociation by UV photons. Our model assumes that PAHs are formed solely through bottom-up processes and does not consider any top-down formation. However, the relatively flat relationship between size and column density for PAHs detected in TMC-1 CP (Wenzel et al. 2025) may indicate that top-down processes are operative. If so, relationship between the C/O ratio and PAH abundances could be significantly different than that presented here, although the contributions of these two scenarios in dense clouds are still unclear.

It is also possible that information regarding the elemental abundances of carbon and oxygen could be extracted by comparison to abundances that are expected to be insensitive to the C/O ratio. H_2CO is the least-sensitive carbon-bearing molecule to the C/O

ratio that has been detected in the ISM, where it has been observed toward many objects (Snyder et al. 1969; Zuckerman et al. 1970; Dieter 1973; Mangum et al. 2008). Although gas-phase formation is more efficient at lower C/O ratios due to the greater availability of oxygen atoms, grain-surface formation via hydrogenation of CO becomes faster at larger C/O ratios due to an increased abundance of CO on grain surfaces. Conversely, cyanopolyyynes have also been widely observed (Turner 1971; Chapillon et al. 2012; Taniguchi et al. 2018; Mendoza et al. 2018; Loomis et al. 2021) but are highly sensitive to the C/O ratio in kinetic models. In Figure 10 the modeled abundances of cyanopolyyynes up to HC_{11}N relative to the modeled abundance of H_2CO are shown as a function of C/O ratio at the time of best fit. Above a C/O ratio of 1, all cyanopolyyynes except HC_{11}N become more abundant than H_2CO with a rapidly increasing abundance ratio. Below a C/O ratio of 1 H_2CO is more abundant, although HC_3N is abundant enough that this ratio is significant and highly influenced by a change to C/O ratio. Given the ubiquity of these species throughout the interstellar medium, the abundance ratios of cyanopolyyynes, particularly HC_3N , to H_2CO might be strong probes of the C/O ratios of astronomical sources.

In terms of major carbon reservoirs, inheritance disk models often consider CO, CO_2 , CH_4 , and occasionally CH_3OH and HCN (Eistrup et al. 2016). This is consistent with previous kinetic models of interstellar ices, in which most of the ice-phase carbon ends up as CO, CO_2 , CH_4 , and CH_3OH (Garrod & Pauly 2011; Aikawa et al. 2020). Likewise, recent JWST observations of molecular cloud ices have found these four molecules to be the most abundant ice-phase carbon reservoirs, although some evidence of complex organic molecules is also seen (Yang et al. 2022; McClure et al. 2023). Our model agrees that CO and CH_4 constitute major carbon reservoirs on interstellar grains. This occurs under all three C/O ratios of 0.5, 1.0, and 2.0, where these species each contain 2% of the total carbon by $\sim 5 \times 10^5$ years and grow in abundance as time progresses until the end of the simulation (10^7 years). However, CO_2 and CH_3OH do not appear as major ice-phase species. Ice-phase CO_2 primarily forms through reaction of CO with OH radicals, which does not become efficient until 12 K and warmer when CO becomes mobile unless non-diffusive mechanisms are invoked (Garrod & Pauly 2011). As our simulation uses a grain temperature of 10 K and does not consider non-diffusive mechanisms, CO_2 is unable to be efficiently formed. Likewise, CH_3OH is typically formed from hydrogenation of CO through successive additions of H atoms; however the first and

third steps to form HCO and CH_3O respectively have been found to have sizable energy barriers (Fuchs et al. 2009). Furthermore, H-atom abstraction to reform HCO is a competing pathway (Hidaka et al. 2009; Chuang et al. 2016) that uses a lower barrier than the addition channels in our model (Ruaud et al. 2015). Conversely, our model does suggest that complex hydrocarbons like C_3H_4 , C_3H_8 , and $\text{CH}_2\text{CHC}_2\text{H}$ can be abundant in ices under oxygen-poor conditions. More work is needed to build a robust, ice chemistry network that can investigate the interplay between formation of simple and complex organic molecules.

In protoplanetary disks, the C/O ratio of the disk and its resulting planets have a strong spatial dependence (Öberg et al. 2011). Detections of complex hydrocarbons such as C_2H_6 , C_3H_4 , and even benzene in inner disks with JWST are challenging the previous, canonical C/O ratio of 0.45. As with molecular clouds like TMC-1 CP, hydrocarbon abundances in chemical kinetic disk models are highly sensitive to the C/O ratio (Öberg et al. 2011; Du et al. 2015; Kanwar et al. 2024), with a large C/O ratio often necessary to reproduce the observed hydrocarbon abundances (Bergin et al. 2016; Kanwar et al. 2024). Additionally, the disk C/O ratio can strongly influence the physics, such as planetesimal formation (Xenos et al. 2025). It is not known whether the initial chemical conditions, such as the presence of molecules and/or an enhanced gas-phase C/O ratio, are inherited from the molecular cloud or if there is a reset back to diffuse cloud, atomic elemental abundances (Eistrup et al. 2016, 2018; Pacetti et al. 2022).

It is possible that such carbon-rich conditions were already present in the previous molecular cloud or that the mechanisms for enhancing carbon relative to oxygen are similar between the cloud and the disk. Since the solar abundance of oxygen is almost two times that of carbon (Lodders 2003), a C/O ratio above unity requires some kind of mechanism that more strongly depletes oxygen. In Furuya et al. (2015), the authors simulate the formation of a molecular cloud to investigate the early-stage water formation. They find that water ice can form quickly even at low visual extinction due to grain-surface hydrogenation of atomic oxygen. As the visual extinction increases and the temperature decreases, desorption of water ice becomes less efficient and the gas-phase abundance of elemental oxygen drops significantly. The formation of gas-phase CO happens on approximately the same timescale. As pointed out by Sellek & Dishoeck (2025), liberation of carbon from CO is also necessary to obtain a C/O ratio above unity. This could be done via reaction with He^+ as they describe and investigate. Alternatively, it is possible that

carbon could be liberated from the processing of carbonaceous grains. For example, [Bocchio et al. \(2014\)](#) calculated the dust lifetime of carbonaceous and silicate grains exposed to interstellar shocks, finding that carbonaceous grains have a shorter lifetime. Another possibility proposed by [Blake et al. \(1987\)](#) is hydrogenation of both C and O on grain surfaces, with the resulting CH₄ being able to desorb much more efficiently than H₂O. Recent work from the GEMS survey studied the relationship between elemental depletion and visual extinction in molecular clouds using observations of molecular emission and chemical modeling ([Fuente et al. 2019](#)). The authors found that within the translucent phase, the gas-phase abundances of carbon and oxygen decrease with visual extinction as they combine to form CO and then CO freezes out onto grains. They also find that a C/O ratio of approximately unity describes their observations of the translucent phase well, requiring an oxygen depletion larger than the “maximum” depletion case of [Jenkins \(2009\)](#). This seemingly corroborates the idea of a greater oxygen depletion in TMC-1 CP, although it is unclear whether the C/O ratio can be further increased above unity.

5. CONCLUSIONS

We explored the effects of varying C/O ratio ranging from 0.1 to 3.0 on modeled hydrocarbon chemistry using the NAUTILUS 3-phase model and a large network containing many complex hydrocarbons, including the PAH naphthalene. Sensitivities of modeled abundances to C/O ratio were determined using relative standard deviation. These depend on the C/O range considered, with unsaturated carbon-chains and bicyclic aromatic molecules being the most affected under astrophysically-relevant conditions. Despite this sensitivity, PAH abundances cannot be reproduced by increasing the C/O ratio. The major carbon reservoirs were visualized using machine learning embedding and dimensionality reduction techniques. These instead consist of simple grain species including CO, CH₄, H₂CO, HCN, and CH₃NH₂ at both low and high C/O ratios. At C/O ratios above unity, there is a significant enhancement of complex hydrocarbon chemistry and the formation of unsaturated carbon-chains. The large abundances of C₃H_n hydrocarbons demonstrate the importance of these molecules, although the network surrounding these species is not complete. Furthermore, the model struggles to reproduce the gas-phase fraction of carbon based on observations of TMC-1 CP. More work regarding the chemistry of C₃H_n and the role they play in PAH formation, as well as general desorption mechanisms and sources of reactive carbon, is needed. Further investigation is

also required to understand the connection between the chemical conditions and inventory of molecular clouds and planet-forming disks.

6. ACKNOWLEDGEMENTS

We thank Dr. Valentine Wakelam for use of the NAUTILUS v1.1 code. We also thank Dr. Hannah Toru Shay, Dr. Aravindh N. Marimuthu, and Zachary T. P. Fried for helpful discussions regarding the machine learning pipeline as well as Dr. Haley N. Scolati and Dr. Kin Long Kelvin Lee for the pipeline itself. A.N.B. acknowledges support from the National Science Foundation Grant Number 2141064. G.W., M.S.H., and B.A.M. acknowledge support from an Arnold and Mabel Beckman Foundation Beckman Young Investigator Award and from the Schmidt Family Futures Foundation. B.A.M. and C.X. acknowledge support of National Science Foundation grant AST-2205126. The National Radio Astronomy Observatory is a facility of the National Science Foundation operated under cooperative agreement by Associated Universities, Inc. The Green Bank Observatory is a facility of the National Science Foundation operated under cooperative agreement by Associated Universities, Inc.

REFERENCES

Agúndez, M., & Wakelam, V. 2013, Chemical Reviews, 113, 8710, doi: [10.1021/cr4001176](https://doi.org/10.1021/cr4001176)

Aikawa, Y., Furuya, K., Yamamoto, S., & Sakai, N. 2020, The Astrophysical Journal, 897, 110, doi: [10.3847/1538-4357/ab994a](https://doi.org/10.3847/1538-4357/ab994a)

Bergin, E. A. 1995, Ph.D., University of Massachusetts Amherst, United States – Massachusetts. <https://www.proquest.com/docview/304209289/abstract/B3AC91D4CF8F4D68PQ/1>

Bergin, E. A., Du, F., Cleeves, L. I., et al. 2016, The Astrophysical Journal, 831, 101, doi: [10.3847/0004-637X/831/1/101](https://doi.org/10.3847/0004-637X/831/1/101)

Blake, G. A., Sutton, E. C., Masson, C. R., & Phillips, T. G. 1987, The Astrophysical Journal, 315, 621, doi: [10.1086/165165](https://doi.org/10.1086/165165)

Bocchio, M., Jones, A. P., & Slavin, J. D. 2014, Astronomy & Astrophysics, 570, A32, doi: [10.1051/0004-6361/201424368](https://doi.org/10.1051/0004-6361/201424368)

Burkhardt, A. M., Loomis, R. A., Shingledecker, C. N., et al. 2021, Nature Astronomy, 5, 181, doi: [10.1038/s41550-020-01253-4](https://doi.org/10.1038/s41550-020-01253-4)

Byrne, A. N., Xue, C., Cooke, I. R., McCarthy, M. C., & McGuire, B. A. 2023, The Astrophysical Journal, 957, 88, doi: [10.3847/1538-4357/acf863](https://doi.org/10.3847/1538-4357/acf863)

Byrne, A. N., Xue, C., Voorhis, T. V., & McGuire, B. A. 2024, Physical Chemistry Chemical Physics, doi: [10.1039/D4CP03229B](https://doi.org/10.1039/D4CP03229B)

Cernicharo, J., Cabezas, C., Fuentetaja, R., et al. 2024, Astronomy and Astrophysics, 690, L13, doi: [10.1051/0004-6361/202452196](https://doi.org/10.1051/0004-6361/202452196)

Chabot, M., Béroff, K., Dartois, E., Pino, T., & Godard, M. 2019, The Astrophysical Journal, 888, 17, doi: [10.3847/1538-4357/ab584f](https://doi.org/10.3847/1538-4357/ab584f)

Chapillon, E., Dutrey, A., Guilloteau, S., et al. 2012, The Astrophysical Journal, 756, 58, doi: [10.1088/0004-637X/756/1/58](https://doi.org/10.1088/0004-637X/756/1/58)

Chen, L.-F., Li, D., Quan, D., et al. 2022, The Astrophysical Journal, 928, 175, doi: [10.3847/1538-4357/ac5a45](https://doi.org/10.3847/1538-4357/ac5a45)

Chuang, K.-J., Fedoseev, G., Ioppolo, S., van Dishoeck, E., & Linnartz, H. 2016, Monthly Notices of the Royal Astronomical Society, 455, 1702, doi: [10.1093/mnras/stv2288](https://doi.org/10.1093/mnras/stv2288)

Chuang, K.-J., Fedoseev, G., Qasim, D., et al. 2018, The Astrophysical Journal, 853, 102, doi: [10.3847/1538-4357/aaa24e](https://doi.org/10.3847/1538-4357/aaa24e)

Dalgarno, A. 2006, Proceedings of the National Academy of Sciences, 103, 12269, doi: [10.1073/pnas.0602117103](https://doi.org/10.1073/pnas.0602117103)

Dieter, N. H. 1973, The Astrophysical Journal, 183, 449, doi: [10.1086/152238](https://doi.org/10.1086/152238)

Du, F., Bergin, E. A., & Hogerheijde, M. R. 2015, The Astrophysical Journal Letters, 807, L32, doi: [10.1088/2041-8205/807/2/L32](https://doi.org/10.1088/2041-8205/807/2/L32)

Dwek, E., Arendt, R. G., Fixsen, D. J., et al. 1997, The Astrophysical Journal, 475, 565, doi: [10.1086/303568](https://doi.org/10.1086/303568)

Eistrup, C., Walsh, C., & Dishoeck, E. F. v. 2018, Astronomy & Astrophysics, 613, A14, doi: [10.1051/0004-6361/201731302](https://doi.org/10.1051/0004-6361/201731302)

Eistrup, C., Walsh, C., & van Dishoeck, E. F. 2016, Astronomy and Astrophysics, 595, A83, doi: [10.1051/0004-6361/201628509](https://doi.org/10.1051/0004-6361/201628509)

Fehér, O., Tóth, L. V., Ward-Thompson, D., et al. 2016, Astronomy and Astrophysics, 590, A75, doi: [10.1051/0004-6361/201424385](https://doi.org/10.1051/0004-6361/201424385)

Fuchs, G. W., Cuppen, H. M., Ioppolo, S., et al. 2009, Astronomy & Astrophysics, 505, 629, doi: [10.1051/0004-6361/200810784](https://doi.org/10.1051/0004-6361/200810784)

Fuente, A., Navarro, D. G., Caselli, P., et al. 2019, Astronomy & Astrophysics, 624, A105, doi: [10.1051/0004-6361/201834654](https://doi.org/10.1051/0004-6361/201834654)

Furuya, K., Aikawa, Y., Hincelin, U., et al. 2015, Astronomy & Astrophysics, 584, A124, doi: [10.1051/0004-6361/201527050](https://doi.org/10.1051/0004-6361/201527050)

Garrod, R. T., & Pauly, T. 2011, The Astrophysical Journal, 735, 15, doi: [10.1088/0004-637X/735/1/15](https://doi.org/10.1088/0004-637X/735/1/15)

Garrod, R. T., Wakelam, V., & Herbst, E. 2007, Astronomy & Astrophysics, 467, 1103, doi: [10.1051/0004-6361:20066704](https://doi.org/10.1051/0004-6361:20066704)

Graedel, T. E., Langer, W. D., & Frerking, M. A. 1982, The Astrophysical Journal Supplement Series, 48, 321, doi: [10.1086/190780](https://doi.org/10.1086/190780)

Habart, E., Natta, A., & Krügel, E. 2004, Astronomy & Astrophysics, 427, 179, doi: [10.1051/0004-6361:20035916](https://doi.org/10.1051/0004-6361:20035916)

He, J., Shi, J., Hopkins, T., Vidali, G., & Kaufman, M. J. 2015, The Astrophysical Journal, 801, 120, doi: [10.1088/0004-637X/801/2/120](https://doi.org/10.1088/0004-637X/801/2/120)

Herbst, E. 1983, The Astrophysical Journal Supplement Series, 53, 41, doi: [10.1086/190882](https://doi.org/10.1086/190882)

Herbst, E., & Leung, C. M. 1986, Monthly Notices of the Royal Astronomical Society, 222, 689, doi: [10.1093/mnras/222.4.689](https://doi.org/10.1093/mnras/222.4.689)

Hickson, K. M., Wakelam, V., & Loison, J.-C. 2016, Molecular Astrophysics, 3-4, 1, doi: [10.1016/j.molap.2016.03.001](https://doi.org/10.1016/j.molap.2016.03.001)

Hidaka, H., Watanabe, M., Kouchi, A., & Watanabe, N. 2009, The Astrophysical Journal, 702, 291, doi: [10.1088/0004-637X/702/1/291](https://doi.org/10.1088/0004-637X/702/1/291)

Hincelin, U., Wakelam, V., Hersant, F., et al. 2011, *Astronomy & Astrophysics*, 530, A61, doi: [10.1051/0004-6361/201016328](https://doi.org/10.1051/0004-6361/201016328)

Jenkins, E. B. 2009, *The Astrophysical Journal*, 700, 1299, doi: [10.1088/0004-637X/700/2/1299](https://doi.org/10.1088/0004-637X/700/2/1299)

Kalvāns, J., & Silsbee, K. 2022, *Monthly Notices of the Royal Astronomical Society*, 515, 785, doi: [10.1093/mnras/stac1792](https://doi.org/10.1093/mnras/stac1792)

Kanwar, J., Kamp, I., Jang, H., et al. 2024, MINDS. Hydrocarbons detected by JWST/MIRI in the inner disk of Sz28 consistent with a high C/O gas-phase chemistry, arXiv, doi: [10.48550/arXiv.2407.14362](https://doi.org/10.48550/arXiv.2407.14362)

Kanwar, J., Kamp, I., Woitke, P., et al. 2025, MINDS. Strong oxygen depletion in the inner regions of a very low-mass star disk?, arXiv, doi: [10.48550/arXiv.2508.11761](https://doi.org/10.48550/arXiv.2508.11761)

Krenn, M., Häse, F., Nigam, A., Friederich, P., & Aspuru-Guzik, A. 2020, *Machine Learning: Science and Technology*, 1, 045024, doi: [10.1088/2632-2153/aba947](https://doi.org/10.1088/2632-2153/aba947)

Kuiper, T. B. H., Kuiper, E. N. R., Dickinson, D. F., Turner, B. E., & Zuckerman, B. 1984, *The Astrophysical Journal*, 276, 211, doi: [10.1086/161604](https://doi.org/10.1086/161604)

Langer, W. D., & Graedel, T. E. 1989, *The Astrophysical Journal Supplement Series*, 69, 241, doi: [10.1086/191313](https://doi.org/10.1086/191313)

Langer, W. D., Graedel, T. E., Frerking, M. A., & Armentrout, P. B. 1984, *The Astrophysical Journal*, 277, 581, doi: [10.1086/161730](https://doi.org/10.1086/161730)

Lee, K. L. K. 2021, Language models for astrochemistry, Zenodo, doi: [10.5281/zenodo.7559628](https://doi.org/10.5281/zenodo.7559628)

Leung, C. M., Herbst, E., & Huebner, W. F. 1984, *The Astrophysical Journal Supplement Series*, 56, 231, doi: [10.1086/190982](https://doi.org/10.1086/190982)

Lodders, K. 2003, *The Astrophysical Journal*, 591, 1220, doi: [10.1086/375492](https://doi.org/10.1086/375492)

Loison, J.-C., Wakelam, V., & Hickson, K. M. 2014a, *Monthly Notices of the Royal Astronomical Society*, 443, 398, doi: [10.1093/mnras/stu1089](https://doi.org/10.1093/mnras/stu1089)

Loison, J.-C., Wakelam, V., Hickson, K. M., Bergeat, A., & Mereau, R. 2014b, *Monthly Notices of the Royal Astronomical Society*, 437, 930, doi: [10.1093/mnras/stt1956](https://doi.org/10.1093/mnras/stt1956)

Loison, J.-C., Agúndez, M., Wakelam, V., et al. 2017, *Monthly Notices of the Royal Astronomical Society*, 470, 4075, doi: [10.1093/mnras/stx1265](https://doi.org/10.1093/mnras/stx1265)

Loomis, R. A., Burkhardt, A. M., Shingledecker, C. N., et al. 2021, *Nature Astronomy*, 5, 188, doi: [10.1038/s41550-020-01261-4](https://doi.org/10.1038/s41550-020-01261-4)

Mangum, J. G., Darling, J., Menten, K. M., & Henkel, C. 2008, *The Astrophysical Journal*, 673, 832, doi: [10.1086/524354](https://doi.org/10.1086/524354)

Marimuthu, A. N., & McGuire, B. A. 2025, *Journal of Chemical Information and Modeling*, 65, 5424, doi: [10.1021/acs.jcim.5c00516](https://doi.org/10.1021/acs.jcim.5c00516)

McClure, M. K., Rocha, W. R. M., Pontoppidan, K. M., et al. 2023, *Nature Astronomy*, 7, 431, doi: [10.1038/s41550-022-01875-w](https://doi.org/10.1038/s41550-022-01875-w)

McGuire, B. A. 2022, *The Astrophysical Journal Supplement Series*, 259, 30, doi: [10.3847/1538-4365/ac2a48](https://doi.org/10.3847/1538-4365/ac2a48)

McGuire, B. A., Loomis, R. A., Burkhardt, A. M., et al. 2021, *Science*, 371, 1265, doi: [10.1126/science.abb7535](https://doi.org/10.1126/science.abb7535)

Mendoza, E., Lefloch, B., Ceccarelli, C., et al. 2018, *Monthly Notices of the Royal Astronomical Society*, 475, 5501, doi: [10.1093/mnras/sty180](https://doi.org/10.1093/mnras/sty180)

Minissale, M., Congiu, E., & Dulieu, F. 2016a, *Astronomy & Astrophysics*, 585, A146, doi: [10.1051/0004-6361/201526702](https://doi.org/10.1051/0004-6361/201526702)

Minissale, M., Dulieu, F., Cazaux, S., & Hocuk, S. 2016b, *Astronomy & Astrophysics*, 585, A24, doi: [10.1051/0004-6361/201525981](https://doi.org/10.1051/0004-6361/201525981)

Minissale, M., Aikawa, Y., Bergin, E., et al. 2022, *ACS Earth and Space Chemistry*, 6, 597, doi: [10.1021/acsearthspacechem.1c00357](https://doi.org/10.1021/acsearthspacechem.1c00357)

Morton, D. C. 1974, *The Astrophysical Journal*, 193, L35, doi: [10.1086/181625](https://doi.org/10.1086/181625)

Morton, D. C., Drake, J. F., Jenkins, E. B., et al. 1973, *The Astrophysical Journal*, 181, L103, doi: [10.1086/181195](https://doi.org/10.1086/181195)

Navarro-Almaida, D., Le Gal, R., Fuente, A., et al. 2020, *A&A*, 637, A39, doi: [10.1051/0004-6361/201937180](https://doi.org/10.1051/0004-6361/201937180)

Pacetti, E., Turrini, D., Schisano, E., et al. 2022, *The Astrophysical Journal*, 937, 36, doi: [10.3847/1538-4357/ac8b11](https://doi.org/10.3847/1538-4357/ac8b11)

Padovani, M., Galli, D., & Glassgold, A. E. 2009, *Astronomy & Astrophysics*, 501, 619, doi: [10.1051/0004-6361/200911794](https://doi.org/10.1051/0004-6361/200911794)

Pratap, P., Dickens, J. E., Snell, R. L., et al. 1997, *The Astrophysical Journal*, 486, 862, doi: [10.1086/304553](https://doi.org/10.1086/304553)

P. Fried, Z. T., Kelvin Lee, K. L., N. Byrne, A., & A. McGuire, B. 2023, *Digital Discovery*, 2, 952, doi: [10.1039/D3DD00020F](https://doi.org/10.1039/D3DD00020F)

Rodríguez-Baras, M., Fuente, A., Rivière-Marichalar, P., et al. 2021, *Astronomy & Astrophysics*, 648, A120, doi: [10.1051/0004-6361/202040112](https://doi.org/10.1051/0004-6361/202040112)

Rosandi, Y., Urbassek, H. M., Nietiadi, M. L., & Alfaridzi, R. 2024, *Journal of Physics: Conference Series*, 2915, 012006, doi: [10.1088/1742-6596/2915/1/012006](https://doi.org/10.1088/1742-6596/2915/1/012006)

Ruaud, M., Loison, J. C., Hickson, K. M., et al. 2015, *Monthly Notices of the Royal Astronomical Society*, 447, 4004, doi: [10.1093/mnras/stu2709](https://doi.org/10.1093/mnras/stu2709)

Ruaud, M., Wakelam, V., Gratier, P., & Bonnell, I. A. 2018, *Astronomy & Astrophysics*, 611, A96, doi: [10.1051/0004-6361/201731693](https://doi.org/10.1051/0004-6361/201731693)

Ruaud, M., Wakelam, V., & Hersant, F. 2016, *Monthly Notices of the Royal Astronomical Society*, 459, 3756, doi: [10.1093/mnras/stw887](https://doi.org/10.1093/mnras/stw887)

Sainburg, T., McInnes, L., & Gentner, T. Q. 2021, *Neural Computation*, 33, 2881, doi: [10.1162/neco_a.01434](https://doi.org/10.1162/neco_a.01434)

Salyk, C., Yang, Y.-L., Pontoppidan, K. M., et al. 2024, *The Astrophysical Journal*, 974, 97, doi: [10.3847/1538-4357/ad62fe](https://doi.org/10.3847/1538-4357/ad62fe)

Savage, B. D., Cardelli, J. A., & Sofia, U. J. 1992, *The Astrophysical Journal*, 401, 706, doi: [10.1086/172098](https://doi.org/10.1086/172098)

Scolati, H. N., Remijan, A. J., Herbst, E., McGuire, B. A., & Lee, K. L. K. 2023, *The Astrophysical Journal*, 959, 108, doi: [10.3847/1538-4357/ad004c](https://doi.org/10.3847/1538-4357/ad004c)

Sellek, A. D., & Dishoeck, E. F. v. 2025, Chemical transformation of CO in evolving protoplanetary discs across stellar masses: a route to C-rich inner regions, arXiv, doi: [10.48550/arXiv.2507.11631](https://doi.org/10.48550/arXiv.2507.11631)

Shimonishi, T., Nakatani, N., Furuya, K., & Hama, T. 2018, *The Astrophysical Journal*, 855, 27, doi: [10.3847/1538-4357/aaa6a](https://doi.org/10.3847/1538-4357/aaa6a)

Shingledecker, C. N., Tennis, J., Le Gal, R., & Herbst, E. 2018, *ApJ*, 861, 20, doi: [10.3847/1538-4357/aac5ee](https://doi.org/10.3847/1538-4357/aac5ee)

Snell, R. L., Langer, W. D., & Frerking, M. A. 1982, *The Astrophysical Journal*, 255, 149, doi: [10.1086/159813](https://doi.org/10.1086/159813)

Snyder, L. E., Buhl, D., Zuckerman, B., & Palmer, P. 1969, *Physical Review Letters*, 22, 679, doi: [10.1103/PhysRevLett.22.679](https://doi.org/10.1103/PhysRevLett.22.679)

Spitzer, Jr., L., & Tomasko, M. G. 1968, *The Astrophysical Journal*, 152, 971, doi: [10.1086/149610](https://doi.org/10.1086/149610)

Swade, D. A. 1989, *The Astrophysical Journal*, 345, 828, doi: [10.1086/167954](https://doi.org/10.1086/167954)

Taniguchi, K., Saito, M., Sridharan, T. K., & Minamidani, T. 2018, *The Astrophysical Journal*, 854, 133, doi: [10.3847/1538-4357/aaa66f](https://doi.org/10.3847/1538-4357/aaa66f)

Tielens, A. 2008, *Annual Review of Astronomy and Astrophysics*, 46, 289, doi: [10.1146/annurev.astro.46.060407.145211](https://doi.org/10.1146/annurev.astro.46.060407.145211)

Tielens, A. G. G. M., & Hagen, W. 1982, *Astronomy and Astrophysics*, 114, 245. <https://ui.adsabs.harvard.edu/abs/1982A&A...114..245T>

Toru Shay, H., Scolati, H. N., Wenzel, G., et al. 2025, *The Astrophysical Journal*, 985, 123, doi: [10.3847/1538-4357/adc80b](https://doi.org/10.3847/1538-4357/adc80b)

Tsuge, M., Molpeceres, G., Aikawa, Y., & Watanabe, N. 2023, *Nature Astronomy*, 7, 1351, doi: [10.1038/s41550-023-02071-0](https://doi.org/10.1038/s41550-023-02071-0)

Turner, B. E. 1971, *The Astrophysical Journal*, 163, L35, doi: [10.1086/180662](https://doi.org/10.1086/180662)

Wakelam, V., Dartois, E., Chabot, M., et al. 2021, *Astronomy & Astrophysics*, 652, A63, doi: [10.1051/0004-6361/202039855](https://doi.org/10.1051/0004-6361/202039855)

Wakelam, V., Gratier, P., Loison, J.-C., et al. 2024, The 2024 KIDA network for interstellar chemistry, arXiv, doi: [10.48550/arXiv.2407.15958](https://doi.org/10.48550/arXiv.2407.15958)

Wakelam, V., Herbst, E., Bourlot, J. L., et al. 2010, *Astronomy & Astrophysics*, 517, A21, doi: [10.1051/0004-6361/200913856](https://doi.org/10.1051/0004-6361/200913856)

Wakelam, V., Herbst, E., & Selsis, F. 2006, *Astronomy & Astrophysics*, 451, 551, doi: [10.1051/0004-6361:20054682](https://doi.org/10.1051/0004-6361:20054682)

Wakelam, V., Loison, J.-C., Herbst, E., et al. 2009, *Astronomy & Astrophysics*, 495, 513, doi: [10.1051/0004-6361:200810967](https://doi.org/10.1051/0004-6361:200810967)

Wakelam, V., Loison, J. C., Mereau, R., & Ruaud, M. 2017, *Molecular Astrophysics*, 6, 22, doi: [10.1016/j.molap.2017.01.002](https://doi.org/10.1016/j.molap.2017.01.002)

Wakelam, V., Herbst, E., Loison, J.-C., et al. 2012, *The Astrophysical Journal Supplement Series*, 199, 21, doi: [10.1088/0067-0049/199/1/21](https://doi.org/10.1088/0067-0049/199/1/21)

Watt, G. D., Millar, T. J., White, G. J., & Harten, R. H. 1986, *Astronomy and Astrophysics*, 155, 339. <https://ui.adsabs.harvard.edu/abs/1986A&A...155..339W>

Weininger, D. 1988, *Journal of Chemical Information and Computer Sciences*, 28, 31, doi: [10.1021/ci00057a005](https://doi.org/10.1021/ci00057a005)

Wenzel, G., Cooke, I. R., Changala, P. B., et al. 2024a, *Science*, 386, 810, doi: [10.1126/science.adq6391](https://doi.org/10.1126/science.adq6391)

Wenzel, G., Speak, T. H., Changala, P. B., et al. 2024b, *Nature Astronomy*, 1, doi: [10.1038/s41550-024-02410-9](https://doi.org/10.1038/s41550-024-02410-9)

Wenzel, G., Gong, S., Xue, C., et al. 2025, *The Astrophysical Journal Letters*, 984, L36, doi: [10.3847/2041-8213/adc911](https://doi.org/10.3847/2041-8213/adc911)

Xenos, K. O., Bitsch, B., & Andama, G. 2025, *Astronomy & Astrophysics*, 701, A47, doi: [10.1051/0004-6361/202555591](https://doi.org/10.1051/0004-6361/202555591)

Xue, C., Byrne, A. N., Morgan, L., et al. 2025, *The Molecular Inventory of TMC-1 with GOTHAM Observations*, arXiv, doi: [10.48550/arXiv.2509.06256](https://doi.org/10.48550/arXiv.2509.06256)

Yang, Y.-L., Green, J. D., Pontoppidan, K. M., et al. 2022, *The Astrophysical Journal Letters*, 941, L13, doi: [10.3847/2041-8213/aca289](https://doi.org/10.3847/2041-8213/aca289)

Zuckerman, B., Buhl, D., Palmer, P., & Snyder, L. E. 1970, *The Astrophysical Journal*, 160, 485, doi: [10.1086/150449](https://doi.org/10.1086/150449)

Öberg, K. I., Murray-Clay, R., & Bergin, E. A. 2011, *The Astrophysical Journal Letters*, 743, L16, doi: [10.1088/2041-8205/743/1/L16](https://doi.org/10.1088/2041-8205/743/1/L16)